The Open Civil Engineering Journal
DOI: 10.2174/0118741495280060240221093636, 2024, 18, e18741495280060

ISSN: 1874-1495
1

MINI-REVIEW ARTICLE **OPEN ACCESS**

Stone Mastic Asphalt Modified With Nano Titanium Dioxide And Potential Exposure To Blast Load: A Review

Nur Syafiqah Shamimi Mohd Zali[1,*], Khairil Azman Masri[1] and Mazlan Abu Seman[1]

[1]*Faculty of Civil Engineering Technology, Universiti Malaysia Pahang Al-Sultan Abdullah, Pahang, Malaysia*

Abstract:
This article states the modification of stone mastic asphalt with nano titanium dioxide and the advantage it has over conventional asphalt. The transport infrastructures must meet the needs of transport as well as other requirements like resilience and multi-hazard resistance in order to satisfy society's desire for sustainable development. Hence, blast load is introduced in this paper as one of the potential hazards that may be exposed to pavements. The use of SMA with nano titanium is believed to impact the pavement's behaviours significantly and can potentially resist higher blast loads and reduce failure in samples. As real field blast tests are limited, a numerical analysis is done to assess the modified pavement's enhancement. The article concludes by recommending using SMA modified with nano titanium as a promising solution to withstand blast loads in pavements.

Keywords: Blast load, Nanomaterials, Stone mastic asphalt, Titanium dioxide, Traffic, Nano titanium.

*Address correspondence to this author at the Faculty of Civil Engineering Technology, Universiti Malaysia Pahang Al-Sultan Abdullah, Pahang, Malaysia; E-mail: syafiqahshamimi@gmail.com

Cite as: Zali N, Masri K, Abu Seman M. Stone Mastic Asphalt Modified With Nano Titanium Dioxide And Potential Exposure To Blast Load: A Review. Open Civ Eng J, 2024; 18: e18741495280060.
http://dx.doi.org/10.2174/0118741495280060240221093636

Received: November 03, 2023
Revised: January 21, 2024
Accepted: January 23, 2024
Published: ?? ??, 2024

1. INTRODUCTION

The pavement industry has continued to grow, but common issues such as rutting, cracking, potholes, and moisture susceptibility still persist. Malaysia's climate, which is characterized by high temperatures, with an annual average temperature of 28°C and a maximum air temperature of 45°C, can increase these issues [1]. Various methods have been applied to the pavement mix to improve its stability, service life, and resistance to permanent deformations [2]. There are also monsoon seasons, and when it passes, the pavement has more visible deformations. Other than normal usage intended for pavements, there are also several usages such as military-related structures, explosion-exposed buildings, airport pavement, and many more [3]. Since the load applied to this kind of pavement is different or relatively higher compared to the normal pavement usage for normal vehicles, these pavements exposed to blast loads have different requirements. The current pavement system is only designed for high loads but has not been exposed to blast loads. Hence, the usage of materials for a new pavement system is introduced to produce a more enhanced multi-layer pavement to resist loads with higher intensity of loads. Nanomaterials are small in size, which makes them easy to employ because the small particle size can impact the asphalt mix and improve its attributes. Nanomaterials are chemical compounds or substances manufactured and used on a micron size. Nanomaterials range in size from 1 to 100 nanometres (nm) [4]. Nanomaterials, such as zinc oxide, titanium dioxide, copper oxide, and silica, have previously found applications in medical, cosmetic, and biological fields, but they are now being introduced to the pavement industry [5]. Nanomaterials are particularly attractive as additives for pavement materials due to their microscopic scale and significant surface area, which give them unique properties when incorporated in the appropriate amounts. There are two methods commonly used to produce nanomaterials: the “top-down” and “bottom-up”

approaches [6]. There are two approaches to the top-down approach. The first strategy involves shrinking larger structures to the nanoscale, while the second involves deconstructing them into their composite pieces [7]. Nanomaterials have diverse properties depending on their type; their positive impact motivates researchers to learn more about them. For example, certain asphalt mix pavement with nanomaterials added to it as a modifying agent and stabilizer has greatly enhanced the qualities of the mix.

2. CHARACTERISTICS OF STONE MASTIC ASPHALT

Flexible and rigid pavements are two distinct types of pavements that are selected based on the characteristics of the road and specific project requirements, these pavements are often found and adjusted according to respective needs [8, 9]. In flexible asphalt typically, three types of flexible asphalt are encountered: dense-graded asphalt, open-graded asphalt and polymer-modified asphalt. The surfacing material for flexible pavements is asphalt [10]. It consists primarily of aggregates and a bituminous binder. The asphalt surface layer and subgrade make up the majority of the flexible pavement structure [11]. The subgrade plays a crucial role in supporting the pavement structure and dissipating the forces generated by traffic. Furthermore, in a flexible composite pavement, all of the structural layers are fully interconnected from the outset [12]. In contrast, concrete pavements are often favoured for the construction of durable roadways due to their ability to distribute loads evenly over the subgrade and their relatively lower structural depth requirements when compared to flexible asphalt pavements [13]. Stone mastic asphalt is an asphalt mix that is classified as gap-graded due to the presence of two main components: a coarse aggregate that makes up most of the mix and a large volume of bitumen acting as the filler [14]. This asphalt mix is different from others because it has a higher content of coarse aggregates that are not uniformly graded. Due to this composition, SMA is able to bear heavy wheel loads more efficiently compared to conventional pavement [15]. To prevent issues such as bleeding in the mix, SMA incorporates an additional additive, such as cellulose fibre, alongside its high bitumen content [16]. Furthermore, the use of coarse aggregate in SMA increases the amount of stone-on-stone contact, resulting in a more durable and long-lasting pavement than traditional designs [17]. Stone mastic asphalt has several advantageous properties, such as high-temperature stability and greater wear resistance. The material possesses enhanced adhesion to prevent particle separation and greater flexibility, even in low temperatures [14]. Although SMA is famous for its strength and durability, it still possesses some disadvantages like rutting, binder drain-down and moisture susceptibility due to its gap-graded structure [18]. Rutting in the stone mastic asphalt mixture typically initiates with an incipient deformation in the bottom level of the mix and progresses to the formation of more cracks with prolonged time, which finally link and cause rutting at the top level of the road. Vehicle loading adds to the production of cracking because the load exceeds the capacity of the pavement, and the capability of it declining with the increase of cracks [19]. These could eventually lead to another problem: water sensitivity. Moisture sensitivity or resistance occurs when moisture slips into existing spaces, gradually weakening and gradually disconnecting the aggregates and bitumen adhesion [20]. Materials, construction, traffic, and the environment can influence road performance and the resulting distress. These factors can be interdependent and affect the pavement's overall quality [21]. Thus, adding stabilizers, additives, or binder modification exists to counter these problems mentioned. For this research, stone mastic asphalt is used alongside nano titanium dioxide. Nano titanium modified binder is added to stone mastic asphalt, which is comprised of coarse aggregates and bitumen, forming a skeleton-like structure. The mechanical properties of this mixture were assessed, and it was discovered that the viscoelastic strain, moisture susceptibility, resilient modulus and binder drain-down aspects of mixture were enhanced. Furthermore, the addition of nano titanium was found to boost engineering properties of the SMA.

In the case of the Public Work Department specification, it specifies the use of 60/70 penetration grade bitumen for SMA mixes [22]. This means that the bitumen used in the mix has a penetration value of 60-70 dmm at 25°C. This grade of bitumen is commonly used in SMA mixes and is known to provide good performance in regard to resistance to deformation and cracking. The chosen binder content is 6.16%, adopted from work by previous studies [23, 24]. The binder properties are shown in Table **1**.

Table 1. Binder properties.

Properties	Descriptions
Specific gravity @25°C	1.01/1.06 kg cm^{-3}
Penetration @25°C	60-70 mm
Softening Point @25°C	49-56 °C
Ductility @25°C	100 cm

Note: *UniversitiMalaysiaPahang, LebuhPersiaranTunKhalilYaakob, 26300, Kuantan, Pahang, Malaysia.

The binder undergoes a binder modification process in which a sample of 500g of bitumen of grade 60/70 was mixed with 1% nano titanium dioxide powder for 1 hour. The nano titanium dioxide used was from 1% to 5%. The binder mixer machine was set up at 1500rpm with heat of 160°C.

3. PROPERTIES OF NANO TITANIUM DIOXIDE (NANO TIO_2)

Nano TiO_2 is a type of transition metal oxide, consisting of one titanium atom and two oxygen atoms at its most basic level. Although it makes up only about a small amount of the Earth's crust, it is one of several metal oxides, including iron [25-27]. The synthesis of nano titanium dioxide involves using the sol-gel method, resulting in a material with self-cleaning and self-

sanitizing capabilities due to its active photo-catalytic properties [28]. Nano TiO_2 has an octahedral basic structure with three TiO_2 crystal structures (TiO_6). The arrangement and linkages of the structure of nano titanium dioxide vary with temperature and can be either spherical or ellipsoidal [29]. Three primary types of nano titanium have a band gap of 3.2 eV and possess an octahedral structure. Rutile, with a tetragonal structure and a band gap of 3.00 eV, and brookite, with an orthorhombic structure with a band gap of 3.26 eV, are the other two main types. Table **2** shows the properties of nano titanium dioxide.

Table 2. Properties of nano titanium dioxide.

Properties	Description
Colour	White
Purity	99.9%
Primary Particle Size	20nm
Structure	Anatase, Rutile, Brookite
Melting Point	1843°C
Boiling Point	2972°C
Relative Density at 25°C	4.26g/cm^3

4. BLAST LOAD

Blast load could happen from an explosion or any disturbance that could impact the whole structure or only a specific point. As with earthquake intensity, blast force has been described as the magnitude of an explosion accident's influence on buildings [30]. These loads, however, carry a very high intensity of force and cannot withstand normal pavement. That is why there is a development of multi-layer asphalt pavement incorporating reinforced concrete to withstand the load [31]. These multi-layer pavements are still being researched due to the lack of literature on the materials usage and the additional additive use. However, it is observed that the expanding use of nanomaterials in the pavement provides a chance to enhance the multi-layer pavement subjected to design requirements depending on the material used. Appropriate component material selection and mix proportioning have been shown to generate concrete with significantly higher strength and toughness than traditional ones produced using standard procedures, all while being competitively priced [32]. Unconfined and enclosed explosions are the two types of blast loads. The major group is defined by whether the blast load occurs within or acts on the structure. Unconfined explosions are classed into three forms according to their blast loading: open-air explosions, airborne explosions, and external blasts. Explosions might be completely vented, partially or completely enclosed [33]. In their research, Wu (2018) suggested a field blast test and slab size of 2.8m length for both sides as it is a square slab and 0.275 thickness is recommended to make a sample the same as a laboratory sample. High-Strength Concrete (HSC), Engineered Cementitious Composites (ECC), and asphalt concrete (AC) with geosynthetics xxv (GST) are used since each of the materials have different properties and could influence the new pavement to perform better under exposure to blast load. Despite the use of several material systems, there is a lack of well-established data on their interface properties. Therefore, further testing is necessary to evaluate the contact strength between these layers. The interface strength between the AC and HSC layers was evaluated through the implementation of both direct and tilt table tests. However, due to the high cost and effort involved in field blast testing, numerical simulations of pavement systems exposed to blast loads were found to be more efficient. Additionally, the fundamental parameters required for calibrating the advanced material model were determined through the utilization of dynamic laboratory tests. The advanced material model was first implemented with the Dynamic Increase Factor (DIF) for AC material. The model was then validated through field blast tests, and a 3D numerical model of the multi-layer pavement was created. Through parametric investigations, it was discovered that increasing the thickness of the HSC and ECC, adding steel fiber to the HSC, and improving subsoil ground conditions could assist in fortifying the pavement's ability to withstand blasts. A design diagram for pavement under various explosive charges was ultimately created. It is important to acknowledge that an explosion event typically generates an energy level of approximately 103 kJ/kg of explosive charge weight. Due to differences in loading durations, the impact and blast loads would apply varied strain rates to the material. In most cases, impact load causes a strain rate of 1 to 10 s-1 in the material, whereas blast load causes a strain rate of 103 s-1. The material's dynamic response to blast and impact loads varies due to differences in the intensity and duration of these loads. Given its high energy level and rapid strain rate, the blast load can inflict greater damage to the material compared to the impact load. Consequently, it is necessary to conduct a blast test to ensure that the proposed pavement material can withstand blast loads. However, reproducing blast loads in a laboratory test is challenging. Therefore, a field trial test will be conducted to assess the dynamic response of the proposed pavement under blast stress. This test will also evaluate the performance of the specimens under actual blast conditions. This novel pavement design utilizes the unique properties of all four materials to their full potential. Laboratory and field trial outcomes have demonstrated that this proposed multi-layer pavement design possesses excellent penetration resistance, strength, flexibility, and multi-resistance capabilities. However, due to limitations in cost and availability of field sites, a limited number of field trial tests have taken place. Therefore, numerical modelling should be utilized to examine the impact of various effects on the performance of the proposed multi-layer pavement design

5. BLAST LOAD APPROACH

For blast load, encountered parameters are the size of the concrete slab used, whether square or rectangular [34]. Then, the amount of TNT used and the distance will be projected. The distance between the slab is also considered, as whether the load will be blasted on the

ground or a concrete table will be chosen. Materials used for making the slab and pavement will be taken into consideration. The properties of materials used are important as they affect the final result of the product.

Evaluation tools

Laboratory tests, numerical methods, and simulation techniques are utilized to assess the effects of blast loads [35]. In order to overcome the limitations of conducting field tests on samples exposed to blast loads, laboratory tests are conducted to study the properties of the materials used. Drop weight tests are one such laboratory test, and to enact the real-life blast load on the material, the blast is conducted on a square or rectangular slab. The resulting damage is then observed, and details such as the depth of explosion, slab cracking, damage pattern, and other related variables are recorded. In addition, numerical methods are also used, such as employing applications like AUTODYN and conducting numerical simulations on a 3D model.

In 2014, Wu and Chew conducted a study on a multi-layer pavement system that included three layers: an Asphalt Concrete (AC) layer reinforced with Geogrid (GST), a High Strength Concrete (HSC) layer, and an Engineered Cementitious Composites (ECC) layer. They used the Polyfelt Microgrid MG-100 with a bi-directional tensile strength of 100 kN/m and an aperture size of 7 mm to reinforce the AC layer. The study involved creating and testing two types of pavement slabs: 275mm thick, as shown in Fig. (**1**), and new pavement with 75mm asphalt, 100mm HSC, and 100mm ECC, as shown in Fig. (**2**). To model the system, the researchers used a 3D dynamic numerical model with LSDYNA.

The field blast tests involved subjecting each 2.8m square slab, with a thickness of 0.275m, to a single detonation using a 7.3kg TNT explosive weight placed in the centre of the slab, raised 170mm above its surface. T12 bars were utilized, and installed in both directions on the bottom layer, spaced approximately 350mm apart. The findings of the field blast tests demonstrated that the proposed multi-layer pavement system, which incorporates ECC, HSC, and AC with GST, could significantly enhance the blast resistance of the pavement. The new multi-layer pavement design shows better performance compared to traditional pavement structures. Furhtermore, due to the significant expenses and resources involved in conducting field trial blast tests, it is suggested to conduct simulations.

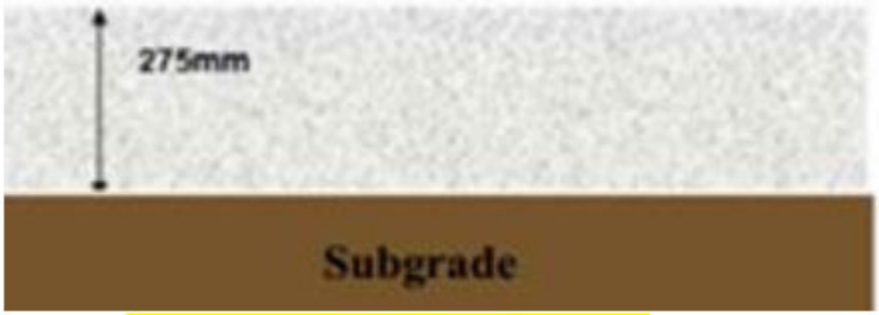

Fig. (1). Normal concrete pavement [37].

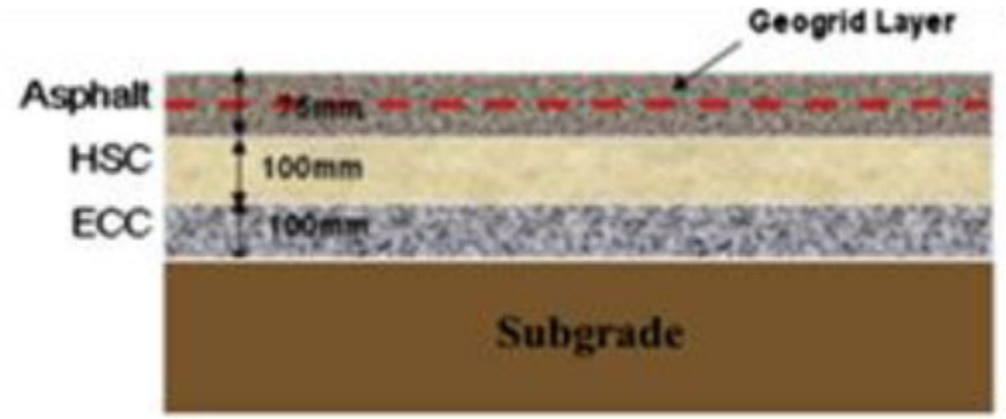

Fig. (2). Composite pavement [37].

Wu *et al*. (2015) conducted research on the performance of cement-based multi-layer composite pavement, specifically the soft-hard-soft (SHS) configuration, against blast load. They cast a slab with dimensions of 2800mm × 800mm × 275mm, which was reinforced with vertical anchors at each corner. The slab consisted of a 75mm thick AC layer on top, followed by a 100mm thick HSC layer, and a 100mm thick ECC layer in the middle, with Geogrid serving as reinforcement for the AC layer. The slab was anchored to the ground, and a field blast test was conducted using a 7.3 kg TNT explosive charge placed approximately 170 mm above the pavement surface.

6. NUMERICAL MODEL FOR BLAST LOAD IN PREVIOUS STUDIES

For 3D modelling, AUTODYN is used to model the blast onto the slab. Significant experimental blast loading gathering of information is challenging due to the high costs, tight regulations, safety issues, and the enormous number of labour needed [36-38]. In the numerical simulation, the materials used must be identified. For example, if the material involved is concrete, air and explosion materials, all the materials must be loaded first into the AUTODYN. Wang *et al*. (2013) used both numerical and experimental methods to compare the damage modes that happened to the concrete after an explosion. In the numerical method, only ¼ of the original slab is considered, and the initial explosion along with the propagation of the wave are modelled. The concrete is under the Lagrange sub-grid, while the air and explosion are under Euler. Euler-Lagrange interaction is considered. The numerical and experimental models shown are reliable even though there are only a few differences that are due to the assumptions considered while inserting data in the numerical model.

The numerical model incorporates air by employing an ideal gas equation of state (EOS), which represents a fundamental and simplified form of EOS. This equation establishes a correlation between pressure and energy. P = (γ - 1) ρe (1) The simulation employs the customary parameters linked to air as defined in the AUTODYN material library, wherein γ is a constant, ρ denotes air density, and e represents specific internal energy, ρ = 1.225 kg/m3, and γ = 14. The initial internal energy of air is considered to be 2.068 × 105 kJ/kg. The Jones-Wilkins-Lee EOS is a common method used to model high explosives like TNT. It describes how the pressure created by the chemical energy released during an explosion affects the system and may be represented as P = A(1-) + B (1-) + (2). In the current simulation, the material constants A, B, R1, R2, and ω for a TNT explosive charge are 3.7377 × 105 MPa, 4.15, 3.747 × 103 MPa, 0.9, and 0.35, respectively. These constants are used to calculate hydrostatic pressure (P), particular volume (V), and specific internal energy (e), where they play an important role. The values for these constants have been obtained through dynamic experiments for various commonly used explosives and are available in AUTODYN. These values are crucial for accurately simulating the behavior of explosives in various scenarios. By inputting these values into the simulation software, researchers can study the effects of different explosive charges and blast scenarios, helping to improve safety and design in areas such as defense, mining, and construction. The values may vary for other types of explosives, and it is important to use the correct values for each specific scenario to ensure accurate results. It is occasionally feasible to skip one or more steps. For example, for a simple analysis, the default solution selections are frequently sufficient. Some steps might be completed out of sequence [7, 39]. The element types and material attributes, for example, can be defined in either order. Loads and boundary conditions can also be defined in either order. It may be required to conduct these steps out of sequence on occasion. According to some studies, decreasing the mesh size has minimal effect on the numerical findings but results in a substantially longer calculation time [40]

7. BLAST LOAD EXPERIMENTAL WORKS

Table **3** shows the shape of the RC panel, which can be rectangular or square, as well as the specimen configuration utilized for the blast test in each of the studies conducted for various reasons.

In a study performed by Wang *et al*. (2013), the deterioration types happened to four samples of the one-way square-reinforced concrete slab were investigated. The slabs were exposed to immediate blast loading resulting from detonations of explosive charges with varying masses. As shown in Fig. (**3**), the slab dimension was 1000 ×1000×40 mm, which has a concrete cover thickness of 20mm. The compressive strength of the concrete cylinders used in the experiment was 39.5MPa. The slabs were secured with steel rigs at two edges using a clamp system. Explosions were induced on the slabs using 0.2-0.55 kg TNT placed 400 mm away from the slabs. As the explosive charge increased, the failure mode of the RC slab shifted from overall flexure to localized punching shear. RC slab C displayed a higher occurrence of radial and circular cracks on the upper side of the slab when subjected to a 0.46kg TNT explosive charge compared to slab B. Among the tested slabs, slab B provided the most accurate prediction, as its simulation results closely matched the experimental results.

Kumar *et al*. (2020) conducted experimental and numerical tests to evaluate the resistance of reinforced concrete slabs to blast loads. The study utilized six C40-grade concrete slabs, reinforced with 10 mm diameter Fe500-grade High Yield Strength Deformed (HYSD) steel bars at a predetermined spacing of 100 mm center to center between two adjacent bars in both directions along the span (Fig. **4**). The slabs were 1000 mm square and 100 mm thick and were subjected to blasts of varying weights, simulating military and terrorist explosives. The slabs were positioned on supports along their two opposing edges, which accurately mimicked the emergency situation given. A calculated amount of Gelatin explosive was located at a standoff distance of either 100 or 500 mm over the slab center using a wooden stand and thread.

Fig. (3). Set up for the test [3].

Table 3. Previous works on blast load.

Specimen Type	Study Description	Specimen Dimension (mm)	Specimen Test Set-up	Numerical	Contribution	Source
Square type	-Doubly reinforced and two-way directions -Subjected to 0.64 kg TNT.	1250×1250×50 (modelled from the previous study) 1000×1000×100 (experimental)	Clamped on steel frame rig	LS-DYNA	It is necessary to examine debris creation after the overpressure has been reduced to zero.	(Wu *et al.*, 2019) [41]
	Three samples are made, two of them are subjected to the explosion at a distance of 0.611 m/kg$^{1/3}$ and one is subjected to blast load at a scaled distance of 0.77 m/kg$^{1/3}$	1000 × 1000 × 40	Mounted on a steel frame hold on both end by U-shape clamps.	LS-DYNA	In both experimental testing and numerical simulations. They shows that the failure patterns of these slabs are split into three types: The comparison reveals that these slabs' failure trend are divided into three types of damage: low, moderate, and severe. The expected and real life results are compatible and shown that blast-proof properties of RCSs can elevated with reinforcement.	(Zhao, Wang, *et al.*, 2019) [42]
	1000 × 1000 × 100	-	ABAQUS	Explosion pressure grew as the amount of TNT increased while decreasing as the standoff distance increased.	1000 × 1000 × 100	-
		1500 × 1500 × 300	Simply supported with four concrete piers holding it.	-	-The BRCS and NRCS have the same spall threshold, but the breaching threshold differs. BRCS also outperform NRCS in terms of anti-blast ability and flexibility. - Current models for predicting concrete damage in close-in explosions are inapplicable to contact explosions, particularly for a thick RC slab. A rewrite of the existing equations is necessary which will aid in the creation of blast-resistant engineering recommendations.	(Yu *et al.*, 2020) [44]
Rectangle type	-Two-way slab with 8mm reinforcement mesh -explosive material composed of a mixture of 50% pentrite and 50% trinitrotoluene (TNT), with a TNT equivalency rating of 1.3.	2170 × 1000 × 100	Clamped on a steel support table	-	Evidence suggests that retrofitting measures can effectively minimize the dispersion of airborne debris and decrease the maximum deflection within the tested range when an explosion occurs.	(Draganić *et al.*, 2021) [43]

Specimen Type	Study Description	Specimen Dimension (mm)	Specimen Test Set-up	Numerical	Contribution	Source
-	-Explosive tests were conducted with TNT at 0.4m standoff distance using three different quantities: 2 kilograms, 4 kilograms, and 6 kilograms.	1000 × 2000 × 120	Steel frame	-	Increasing the charge weight will lead to a greater number of fragments being produced and propelled a further distance. As the charge weight increases,the proportion of small fragments also increases.	-Explosive tests were conducted with TNT at 0.4m standoff distance using three different quantities: 2 kilograms, 4 kilograms, and 6 kilograms.

The distance between the center of the explosive and the top surface of the slab was measured to determine the standoff distance. It is important to note that the quantity of Gelatin explosive used in the experiment was first converted to equivalent TNT by multiplying its weight with the relative effectiveness (R.E.) factor. The R.E. coefficient for Gelatin explosives was found to be 0.62.

Likewise, it is worth noticing that the Gelatin bundle was suspended from its core. The detonation of the Gelatin sticks was observed from the center of the bundle's length, which was positioned parallel to the surface of the slab. To facilitate the detonation wave, the Gelatin sticks were wrapped in a cordex, which acts as a carrier for the wave. For simulations of the current explosive situation, the ABAQUS/Explicit finite element code was employed. This work merely modelled a fourth of the intended reinforced concrete plate/slab (500 mm 500 mm 100 mm), taking advantage of the slab's geometry alignment, supporting layout, support, and loading condition.

Concrete spalling/scabbing has been noticed on the targeted reinforced concrete slabs, crater creation, and crack growth. The slabs were set on the ground; however, no slabs fell off during testing. Various failure types and amounts of blast-induced damage allowed for a better knowledge of the behavior of RC slabs whenever subjected to similar impact/shock from mortars and rocket attacks. The one-way bending of the slab becomes more dominating as the explosive charge increases. The localized failure of the slab, on the other hand, changed into a worldwide deformation as the standoff distance increased. Simulations based on finite elements in ABAQUS/Explicit were used to simulate concrete deterioration, crater formation, and spalling/scabbing. The explosion pressure grew as the amount of TNT increased while the explosion pressure when the standoff distance increased, decreases.

Zhao *et al*. (2019) carried out tests to assess the explosive behaviors of small-scale reinforced concrete slabs (RCS) in terms of experimental and numerical. The dimension of the slab of 1000 mm × 1000 mm × 40 mm was used with a concrete grade of C30 with a concrete cover of about 16mm. The reinforcement bars (RB) were applied in a single mesh layer with a diameter of 8mm or 6mm. Three small-scale RCSs were cured; two RCSs were subjected to the explosion at a distance of 0.611 m/kg1/3, while the third RCS was exposed to blast load at a distance of 0.77 m/kg1/3. The slab was clamped with 10 U-shape clamp loops at the opposite two sides and under it lies a steel frame.

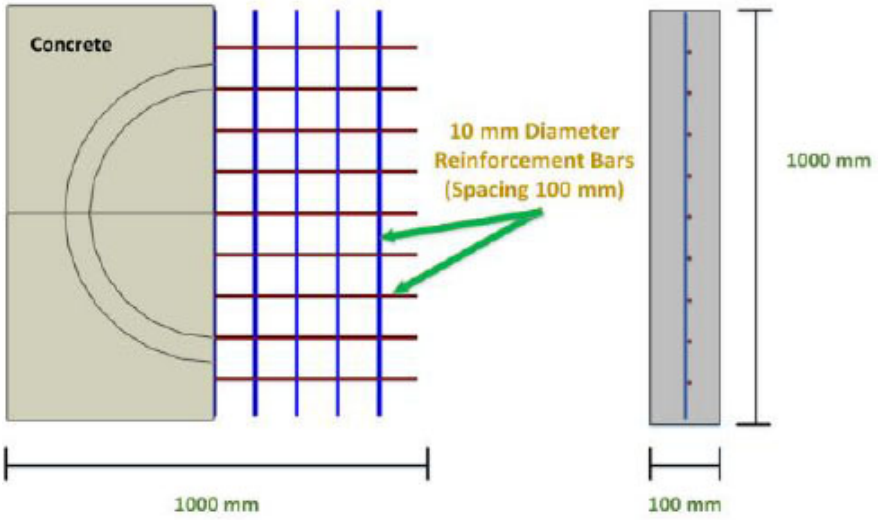

Fig. (4). Slab dimension with bars [45].

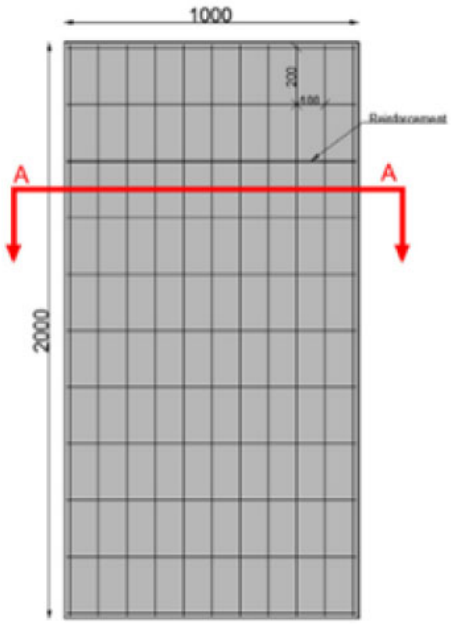

Fig. (5). Slab dimension (mm) [47].

Three small-scale RCSs were cured; two RCSs had been subjected to an explosion at 0.611 m/kg$^{1/3}$, while the third one was exposed to an explosion at 0.77 m/kg$^{1/3}$. The slab was secured with 10 U-shaped clamp loops on the opposite two sides, and a steel frame was installed beneath it.

Punching flexural failure, global flexural failure, and punching failure: damage modes were derived through testing and numerical simulation.

As the reinforcing ratio and explosive charges grow, the highest displacement, number of cracks, and degree of damage all decrease. Concrete penetration failure in the middle, major crack spread, and concrete deterioration on the underside were found in RCS with a low reinforcing ratio. Distributed reinforcement bars can considerably improve blast resistance and slab integrity. The highest relative error percentage in the RCSs' damaged zone is less than 15.3%, and the lowest error percentage in the affected zone is 2.43%, which meets the engineering design criterion [44, 45, 31].

In their study, Shi *et al*. (2020) conducted experiments on fragments produced by close-in explosions. The slabs were 2000 mm x 1000 mm in size, with a width of 120 mm, as shown in Fig. (**5**). The slabs were constructed using commercial concrete grade C30 from China and supported on both sides with steel bars of 12mm diameter spaced at a distance of 100 mm for active steel bars and 200 mm for constructional steel bars with 20mm cover. A total of five RC slabs were built in the laboratory, and 2 kg up to 6kg with an interval of 2 of TNT were used.

In this testing, a 1.5-meter-wide, 4-meter-long, and 2.5-meter-high steel holding structure was created to support the RC slabs during the tests. To ensure stability of the RC slab specimen, two channel steels were connected and secured to the steel frame using the test equipment. During the experiments, wooden chocks were used to prevent oscillation of the slabs. Additionally, two high-strength bolts were firmly inserted into the soil and attached to the frame to prevent it from moving forward due to blast energy. The shaped TNT charge, which had a density of 1630 kg/m^3, was hung in front of the specimen. The charges were then detonated at a distance of 0.4m from the bottom towards the center of the slabs [46]. This study suggests that adopting strategies like increasing reinforcement and protection distance can be helpful in mitigating the danger regarding fragments. The likelihood of focused damage, such as deterioration and breaking, is higher in remote explosions compared to general flexural or shear damage. In the case of TNT charges weighing 6 kg, the maximum velocity of ejected pieces from RC slabs due to close-in blast pressures can reach as high as 100 m/s.

In their research, Draganić *et al*. (2020), and Luccioni *et al*. (2006) [43, 47, 48] examined the durability of reinforced concrete slabs subjected to blast loads. They modified the slabs using glass fiber textiles impregnated with epoxy resin. The slabs were 2170 × 1000, had a thickness of 100mm, and were reinforced with a two-way mesh measuring 8 mm. A 1.5 cm protective layer was also added, resulting in a 7 cm separation between the compressive and tensile reinforcing mesh layers. The steel grade used was B500, and the concrete grade was C20/25.

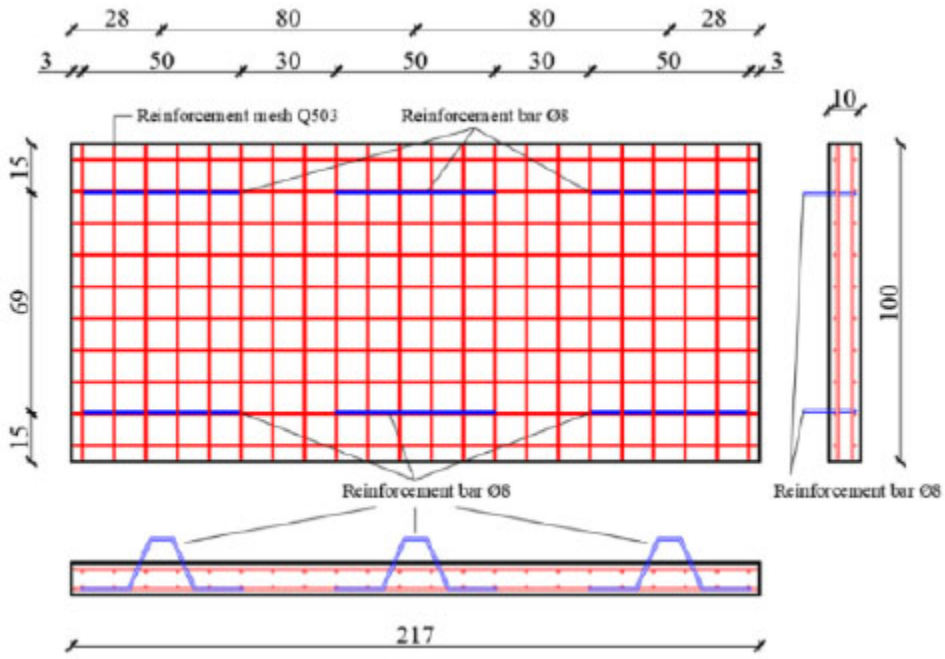

Fig. (6). Sample dimension [43].

Two types of glass fiber textiles with epoxy glue reinforcement were used to create composite retrofit systems, including glass woven cloth and chopped strand glass mats. Twelve slabs were evaluated, with 9 being modified and 3 left unmodified. Four of them were tested, one as a reference and three modified with designed composite systems. The arrangement for static load tests included two plates of steel for support, a steel response frame, and a steel force application frame, as shown in Fig. (**6**). To create a four-point bending test and replicate simply supported boundary conditions, Teflon plates were inserted between the slab and four steel point supports. Additionally, a specially designed steel hinge was utilized to connect the hydraulic jack to both the response and the force application steel frame. These loads inflicted on the surface have different reactions and the amount of load they could manage is observed [49].

These previous researchers investigated the slab component and the damages that happen under blast load through field test and numerical tests but there is a concern with how blast load will affect a different type of structure like pavement. Since pavement is said to be more vulnerable under the threat of explosion accidents. Hence, by modifying the pavement with nano titanium dioxide, it is hopeful that the findings from the testing could add to the idea of anti-blasting pavement.

CONCLUSION

This paper is a mini review on the nano modification on stone mastic asphalt with an insight into blast load. This review intends to see the blast load effect on the pavement structure. By looking at some effect the blast load has on concrete structures when making a new pavement, researchers can include a material that is sufficient to cater to high loads. The ideas from this review will be a good idea for future researchers that have an interest in anti-blasting pavement. The thought from this research could add to the findings for future design purposes.

LIST OF ABBREVIATIONS

HSC	=	High-Strength Concrete
ECC	=	Engineered Cementitious Composites
AC	=	Asphalt Concrete

CONSENT FOR PUBLICATION

Not applicable.

AVAILABILITY OF DATA AND MATERIALS

The data supporting the findings of the article is available in the (Zenodo Repository) at https://zenodo.org/me/requests/fc5604eb-b80a-4983-872a-fdbb9e6ea9a5, reference number (10.5281/zenodo.10730368).

FUNDING

This study was funded by UNIVERSITI MALAYSIA PAHANG AL-SULTAN ABDULLAH (UMPSA), Awards/Grant number. PDU213206.

CONFLICT OF INTEREST

The authors declare no conflict of interest, financial or otherwise.

ACKNOWLEDGEMENTS

Thank you to University Malaysia Pahang Al-Sultan Abdullah for providing the necessary funds and facilities. Thank you to everyone who contributed to the production of this paper.

REFERENCES

[1] H.Y. Katman, M.R. Ibrahim, M.R. Karim, N.S. Mashaan, and S. Koting, "Evaluation of permanent deformation of unmodified and rubber-reinforced SMA asphalt mixtures using dynamic creep test", *Adv. Mater. Sci. Eng,* vol. 2015, 2015.

[2] R. Babagoli, "Laboratory investigation of the performance of binders and asphalt mixtures modified by carbon nano tube, poly phosphoric acid, and styrene butadiene rubber", *Constr. Build. Mater.,* vol. 275, p. 122178, 2021. [http://dx.doi.org/10.1016/j.conbuildmat.2020.122178]

[3] W. Wang, D. Zhang, F. Lu, S. Wang, and F. Tang, "Experimental study and numerical simulation of the damage mode of a square reinforced concrete slab under close-in explosion", *Eng. Fail. Anal.,* vol. 27, pp. 41-51, 2013. [http://dx.doi.org/10.1016/j.engfailanal.2012.07.010]

[4] P. Caputo, M. Porto, R. Angelico, V. Loise, P. Calandra, and O.C. Rossi, "Bitumen and asphalt concrete modified by nanometer-sized particles: Basic concepts, the state of the art and future perspectives of the nanoscale approach", *Adv. Colloid Interface Sci.,* vol. 285, p. 102283, 2020. [http://dx.doi.org/10.1016/j.cis.2020.102283] [PMID: 33099178]

[5] S.A. Mazari, E. Ali, R. Abro, F.S.A. Khan, I. Ahmed, M. Ahmed, S. Nizamuddin, T.H. Siddiqui, N. Hossain, N.M. Mubarak, and A. Shah, "Nanomaterials: Applications, waste-handling, environmental toxicities, and future challenges – A review", *J. Environ. Chem. Eng.,* vol. 9, no. 2, p. 105028, 2021. [http://dx.doi.org/10.1016/j.jece.2021.105028]

[6] D. Rawtani, P.K. Rao, and C.M. Hussain, "Recent advances in analytical, bioanalytical and miscellaneous applications of green nanomaterial", *Trends Analyt. Chem.,* vol. 133, p. 116109, 2020. [http://dx.doi.org/10.1016/j.trac.2020.116109]

[7] J. Zhou, T. Yang, J. Chen, C. Wang, H. Zhang, and Y. Shao, "Two-dimensional nanomaterial-based plasmonic sensing applications: Advances and challenges", *Coord. Chem. Rev.,* vol. 410, no. 5, p. 213218, 2020.

[8] P.K. Gautam, P. Kalla, A.S. Jethoo, R. Agrawal, and H. Singh, "Sustainable use of waste in flexible pavement: A review", *Constr. Build. Mater.,* vol. 180, pp. 239-253, 2018. [http://dx.doi.org/10.1016/j.conbuildmat.2018.04.067]

[9] P. Solanki, and M. Zaman, "Design of semi-rigid type of flexible pavements", *Int. J. Pavement Res. Technol.,* vol. 10, no. 2, pp. 99-111, 2017. [http://dx.doi.org/10.1016/j.ijprt.2016.10.004]

[10] C. Maduabuchukwu, S. Poh, and C. Wah, "Laboratory study on recycled concrete aggregate based asphalt mixtures for sustainable flexible pavement surfacing", *J. Clean. Prod.,* vol. 262, p. 121462, 2020.

[11] J. Peng, J. Zhang, J. Li, Y. Yao, and A. Zhang, "Modeling humidity and stress-dependent subgrade soils in flexible pavements", *Comput Geotech.,* vol. 120, p. 103413, 2020.

[12] L. You, J. Man, K. Yan, D. Wang, and H. Li, "Combined fourier-wavelet transforms for studying dynamic response of anisotropic multi-layered flexible pavement with linear-gradual interlayers", *Appl. Math. Model.,* vol. 81, pp. 559-581, 2020.

[13] A. Alsaif, R. Garcia, F.P. Figueiredo, K. Neocleous, A. Christofe, M. Guadagnini, and K. Pilakoutas, "Fatigue performance of flexible steel fibre reinforced rubberised concrete pavements", *Eng. Struct.,* vol. 193, pp. 170-183, 2019. [http://dx.doi.org/10.1016/j.engstruct.2019.05.040]

[14] A. Chegenizadeh, L. Tokoni, H. Nikraz, and E. Dadras, "Effect of ethylene-vinyl acetate (EVA) on stone mastic asphalt (SMA) behaviour", *Constr Build Mater.,* vol. 272, p. 121628, 2020. [http://dx.doi.org/10.1016/j.conbuildmat.2020.121628]

[15] M. Irfan, Y. Ali, S. Ahmed, S. Iqbal, and H. Wang, "Rutting and fatigue properties of cellulose fiber-added stone mastic asphalt concrete mixtures", *Adv. Mater. Sci. Eng.,* vol. 2019, 2019.

[16] K.N.L.N. Kumar, and A. Ravitheja, "Characteristics of stone matrix asphalt by using natural fibers as additives", *Mater. Today Proc.,* vol. 19, pp. 397-402, 2019. [http://dx.doi.org/10.1016/j.matpr.2019.07.624]

[17] Y. Liu, Y. Huang, W. Sun, H. Nair, D.S. Lane, and L. Wang, "Effect of coarse aggregate morphology on the mechanical properties of stone matrix asphalt", *Constr. Build. Mater.,* vol. 152, pp. 48-56, 2017. [http://dx.doi.org/10.1016/j.conbuildmat.2017.06.062]

[18] R. Guo, T. Nian, and F. zhou, "Analysis of factors that influence anti-rutting performance of asphalt pavement", *Constr. Build. Mater.,* vol. 254, p. 119237, 2020. [http://dx.doi.org/10.1016/j.conbuildmat.2020.119237]

[19] M. Alinezhad, and A. Sahaf, "Investigation of the fatigue characteristics of warm stone matrix asphalt (WSMA) containing electric arc furnace (EAF) steel slag as coarse aggregate and Sasobit as warm mix additive", *Case Stud. Constr. Mater.,* vol. 11, no. 12, p. e00265, 2019.

[20] A. Ameli, D. Nasr, R. Babagoli, A. Hossein, and N. Norouzi, "Laboratory evaluation of rheological behavior of binder and performance of stone matrix asphalt (SMA) mixtures containing zycotherm nanotechnology, sasobit, and rheofalt warm mixture additives", *Constr Build Mater.,* vol. 262, no. 11, p. 120757, 2020. [http://dx.doi.org/10.1016/j.conbuildmat.2020.120757]

[21] A. Hosseini, A. Faheem, H. Titi, and S. Schwandt, "Evaluation of the long-term performance of flexible pavements with respect to production and construction quality control indicators", *Constr Build Mater.,* vol. 230, no. 1, p. 116998, 2020.

[22] JKR, "JKR/SPJ/2008-S4 standard specification for road works part4 flexible pavement", Available from: https://jkrmarang.terengganu.gov.my/files/Muat%20Turun/Standard_Specification_For_Road_WorksFlexible_Pavement.pdf

[23] A.K. Arshad, E. Shaffie, W. Hashim, F. Ismail, and K.A. Masri, "Evaluation of nanosilica modified stone mastic asphalt", *Int. J. Civ. Eng. Technol.,* vol. 10, no. 2, pp. 1508-1516, 2019.

[24] N.S.M.Z Syafiqah, K.A. Masri, and N.E. Jasni, "Effect of tocilizumab vs usual care in adults hospitalized with COVID-19 and moderate or severe pneumonia: A randomized clinical trial", *JAMA Intern Med,* vol. 181, no. 1, pp. 32-40, 2021.

[25] H. He, J. Hu, R. Li, C. Shen, J. Pei, and B. Zhou, "Study on rheological properties of silica nanofluids modified asphalt binder", *Constr. Build. Mater.,* vol. 273, p. 122046, 2021. [http://dx.doi.org/10.1016/j.conbuildmat.2020.122046]

[26] N.A.N. Md Fauzi, K.A. Masri, P.J. Ramadhansyah, M.S. Samsudin, A. Ismail, A.K. Arshad, E. Shaffie, A.H. Norhidayah, and M.R. Hainin, "Volumetric properties and resilient modulus of stone mastic asphalt incorporating cellulose fiber", *3rd National Conference on Wind & Earthquake Engineering and International Seminar On Sustainable Construction Engineering,* 2020p. 012028 Kuala Lumpur, Malaysia

[27] N A M. Radzi, K.A. Masri, P.J. Ramadhansyah, N.E. Jasni, A.K. Arshad, J. Ahmad, N. Mashros, and H. Yaacob, "Stability and resilient modulus of porous asphalt incorporating steel fiber", *3rd National Conference on Wind & Earthquake Engineering and International Seminar On Sustainable Construction Engineering,* p. 012027 Kuala Lumpur, Malaysia

[28] Z.N. Jameel, O.A. Mahmood, and F.L. Ahmed, "Studying the effect of synthesized nano-titanium dioxide via two phases on the pseudomonas aeruginosa and portus bacteria as antimicrobial agents", *Int. J. Nanoelectron. Mater.,* vol. 12, no. 3, pp. 329-338, 2019.

[29] Z. Li, S. Ding, X. Yu, B. Han, and J. Ou, "Multifunctional cementitious composites modified with nano titanium dioxide: A review", *Compos., Part A Appl. Sci. Manuf.,* vol. 111, no. May, pp. 115-137, 2018.

[http://dx.doi.org/10.1016/j.compositesa.2018.05.019]
[30] X. Zhang, Z. Li, Y. Shi, C. Wu, and J. Li, "Fragility analysis for performance-based blast design of FRP-strengthened RC columns using artificial neural network", *J. Build. Eng.,* vol. 52, no. 11, p. 104364, 2022.
[http://dx.doi.org/10.1016/j.jobe.2022.104364]
[31] J. Wu, X. Liu, and S.H. Chew, "Parametric study on cement-based soft-hard-soft (SHS) multi-layer composite pavement against blast load", *Constr. Build. Mater.,* vol. 98, pp. 602-619, 2015.
[http://dx.doi.org/10.1016/j.conbuildmat.2015.08.046]
[32] J. Wu, H. Wu, H.W.A. Tan, and S.H. Chew, *Multi-layer Pavement System Under Blast Load.,* Springer: Singapore, 2018.
[http://dx.doi.org/10.1007/978-981-10-5001-5]
[33] M.A. Seman, S.S.M. Mohsin, and Z.M. Jaini, "Blast load assessment: RC wall subjected to blast load", *IOP Conf. Ser.: Earth Environ. Sci.,* vol. 244, p. 012007, 2019.
[http://dx.doi.org/10.1088/1755-1315/244/1/012007]
[34] C. Zhao, X. Lu, Q. Wang, A. Gautam, J. Wang, and Y. L. Mo, "Mild or moderate Covid-19", *N Engl J Med,* vol. 383, no. 18, pp. 1757-1766, 2020.
[http://dx.doi.org/10.1016/j.engstruct.2019.109337]
[35] A.K. Gomathi, A. Rajagopal, and S.S. Prakash, "Predicting the failure mechanism of RC slabs under combined blast and impact loading", *Theor. Appl. Fract. Mech.,* vol. 119, no. March, p. 103357, 2022.
[http://dx.doi.org/10.1016/j.tafmec.2022.103357]
[36] J. Wu, and S.H. Chew, "Field performance and numerical modeling of multi-layer pavement system subject to blast load", *Constr. Build. Mater.,* vol. 52, pp. 177-188, 2014.
[http://dx.doi.org/10.1016/j.conbuildmat.2013.11.035]
[37] W. Xiao, M. Andrae, M. Steyerer, and N. Gebbeken, "Investigations of blast loads on a two-storeyed building with a gable roof: Full-scale experiments and numerical study", *J. Build. Eng.,* vol. 43, no. August, p. 103111, 2021.
[http://dx.doi.org/10.1016/j.jobe.2021.103111]
[38] M.K. Almustafa, and M.L. Nehdi, "Machine learning prediction of structural response for FRP retrofitted RC slabs subjected to blast loading", *Eng. Struct.,* vol. 244, no. July, p. 112752, 2021.
[http://dx.doi.org/10.1016/j.engstruct.2021.112752]
[39] J. Shin, and J.S. Jeon, "Retrofit scheme of FRP jacketing system for blast damage mitigation of non-ductile RC building frames", *Compos. Struct.,* vol. 228, no. August, p. 111328, 2019.
[http://dx.doi.org/10.1016/j.compstruct.2019.111328]
[40] Y. Shi, and M.G. Stewart, "Damage and risk assessment for reinforced concrete wall panels subjected to explosive blast loading", *Int. J. Impact Eng.,* vol. 85, pp. 5-19, 2015.
[http://dx.doi.org/10.1016/j.ijimpeng.2015.06.003]
[41] Z. Wu, P. Zhang, L. Fan, and Q. Liu, "Debris characteristics and scattering pattern analysis of reinforced concrete slabs subjected to internal blast loads–A numerical study", *Int. J. Impact Eng.,* vol. 131, pp. 1-16, 2019.
[http://dx.doi.org/10.1016/j.ijimpeng.2019.04.024]
[42] C. Zhao, Q. Wang, X. Lu, X. Huang, and Y.L. Mo, "Blast resistance of small-scale RCS in experimental test and numerical analysis", *Eng. Struct.,* vol. 199, no. May, p. 109610, 2019.
[http://dx.doi.org/10.1016/j.engstruct.2019.109610]
[43] H. Draganić, G. Gazić, S. Lukić, and M. Jeleč, "Experimental investigation on blast load resistance of reinforced concrete slabs retrofitted with epoxy resin impregnated glass fiber textiles", *Compos. Struct.,* vol. 274, no. 12, p. 114349, 2021.
[http://dx.doi.org/10.1016/j.compstruct.2021.114349]
[44] X. Yu, B. Zhou, F. Hu, Y. Zhang, X. Xu, C. Fan, W. Zhang, H. Jiang, and P. Liu, "Experimental investigation of basalt fiber-reinforced polymer (BFRP) bar reinforced concrete slabs under contact explosions", *Int. J. Impact Eng.,* vol. 144, no. February, p. 103632, 2020.
[http://dx.doi.org/10.1016/j.ijimpeng.2020.103632]
[45] V. Kumar, K. V Kartik, and M. A. Iqbal, "Experimental and numerical investigation of reinforced concrete slabs under blast loading", *Eng. Struct.,* vol. 206, no. 10, p. 110125, 2020.
[http://dx.doi.org/10.1016/j.engstruct.2019.110125]
[46] > "*Development of advanced pavement materials system for blast load*", ScholarBank@NUS Repository, 2012.
[47] Y. Shi, J. Wang, and J. Cui, "Experimental studies on fragments of reinforced concrete slabs under close-in explosions", *Int. J. Impact Eng.,* vol. 144, p. 103630, 2020.
[http://dx.doi.org/10.1016/j.ijimpeng.2020.103630]
[48] B.M. Luccioni, and M. Luege, "Concrete pavement slab under blast loads", *Int. J. Impact Eng.,* vol. 32, no. 8, pp. 1248-1266, 2006.
[http://dx.doi.org/10.1016/j.ijimpeng.2004.09.005]
[49] H. Draganić, D. Varevac, and S. Lukić, "An overview of methods for blast load testing and devices for pressure measurement", *Adv. Civ. Eng.,* vol. 2018, pp. 1-20, 2018.
[http://dx.doi.org/10.1155/2018/3780482]